Published in final edited form as:
Science. 2010 August 27; 329(5995): 1071–1075. doi:10.1126/science.1187292.

Crystal structure of human adenovirus at 3.5 Å resolution*

Vijay S. Reddy[1,§], **S. Kundhavai Natchiar**[1], **Phoebe L. Stewart**[2], and **Glen R. Nemerow**[1,§]
[1]The Scripps Research Institute, 10550 North Torrey Pines Road, La Jolla, CA 92037
[2]Vanderbilt University Medical Center, 2215 Garland Avenue, 710 Light Hall, Nashville, TN, 37232

Abstract

Rational development of adenovirus vectors for therapeutic gene transfer is hampered by the lack of accurate structural information. Here we report the X-ray structure at 3.5 Å resolution of the 150 megadalton adenovirus capsid containing nearly 1 million amino acids. We describe interactions between the major capsid protein (hexon) and several accessory molecules that stabilize the capsid. The virus structure also reveals an altered association between the penton base and the trimeric fiber protein, perhaps reflecting an early event in cell entry. The high-resolution structure provides a significant advance towards understanding the assembly and cell entry mechanisms of a large dsDNA virus and provides new opportunities for improving adenovirus-mediated gene transfer.

Human adenoviruses (HAdV) are non-enveloped dsDNA viruses that are associated with acute infections (1–3). While these infections are generally self-limiting, the re-emergence of certain HAdV types has also been linked to potentially fatal respiratory infections in both civilian and military populations (4). Severe disseminated diseases also occur in patients receiving bone marrow-derived stem cells (5,6). In addition to their disease associations, replication-defective or conditionally replicating HAdVs continue to be evaluated in ~25% of approved Phase I–III clinical trials for vaccine and therapeutic gene transfer (7,8). However, the lack of accurate details of the virus structure limits the re-engineering of HAdV vectors and prevents a better understanding of the virus life cycle. High resolution HAdV structure determination presents a challenge because of the large size (910 Å ave. dia., 150 MDa) and complexity (*pseudo*-T=25) of the virus. The crystal structures of the major HAdV capsid proteins; the fiber (9), penton base (PB) (10) and hexon (11) have been solved. The hexon and penton base crystal structures were subsequently used to derive *pseudo*-atomic models of the HAdV capsid at moderately high resolution (7–10 Å) (12–14) by cryoelectron microscopy (cryoEM). CryoEM structural analyses provided considerable insight into HAdV organization; however, they did not furnish detailed information on the interactions between the major and accessory (cement) proteins (IIIa,VI,VIII, and IX).

We report here the crystal structure of a recombinant HAdV-5 vector, designated Ad35F, that is equipped with a short and flexible fiber protein derived from HAdV-35 (15). Details of the crystallization (16), diffraction data statistics (Table S1) and structure determination of Ad35F at near atomic resolution (3.5 Å) are described in the Methods (17).

The architecture of the HAdV capsid is shown in Fig. 1a, b. The hexon is the most abundant protein in the capsid with 720 subunits arranged as 240 trimers on a *pseudo*-T=25 icosahedral

§To whom correspondence should be addressed. gnemerow@scripps.edu (G.R.N.); reddyv@scripps.edu (V.S.R.).

Supporting Online Material www.sciencemag.org Methods Figures S1, S2, S3, S4, S5 and S6 Table S1

lattice. Five penton base (PB) monomer subunits occupy each of the icosahedral vertices and are associated with the trimeric fiber protein. Each of the 20 facets of the capsid contains 12 hexon trimers and a penton at each vertex. The icosahedral asymmetric unit consists of 4 hexon trimers and one PB monomer. As previously described, each hexon monomer contains two eight-stranded jellyroll domains, V1 and V2 (11), while the PB subunit contains a single jellyroll domain (10). Three sets of V1 and V2 domains give the hexon trimer a *pseudo*-hexagonal shape at the base, which in turn gives rise to a *pseudo*-T=25 architecture for the HAdV capsid. Large insertions between the strands of the hexon jellyroll domains form triangular towers on top of the hexagonal base. Representative electron density for a hexon subunit (aa 579–582) is shown in Fig. S1. Some of the hypervariable region loops (aa 186–193, 250–258) that were disordered in the isolated hexon structure are visible in the HAdV capsid crystal structure (Fig. S1), as they are involved in multiple, symmetry-related inter-hexon contacts (Fig. S2, S3). The tertiary structures of the 12 structurally independent hexon subunits are virtually identical having an r.m.s.d. of ~1 Å upon superposition with a few differences found mainly at the amino and carboxy termini.

An unusual molecular interaction in the HAdV particle occurs between the 5-fold symmetric PB and the 3-fold symmetric fiber protein. The “symmetry mismatch” that occurs between the PB and fiber is of particular interest because of its potential impact on cell receptor interactions as well as subsequent disassembly processes. Previous cryoEM structural analyses of HAdV at moderate resolution and a co-crystal structure of PB with an N-terminal fiber peptide suggested that the fiber protein interacts on the outer surface of the PB (18,19). Consistent with this model, the crystal structure of recombinant PB alone (Fig. 2) indicated that the central pore of the PB pentamer is too narrow to allow fiber insertion (10). However, in the Ad35F particle the central pore of the PB has nearly twice the diameter as that of the isolated (fiberless) PB (10) (Fig. 2b). Hence, the dimensions for the PB pore in the Ad35F structure but not in the isolated PB would allow insertion of the fiber shaft domain into the central cavity of the PB. Consistent with this, Fig. 2c, d shows strong F_o-F_c electron density along the icosahedral 5-fold symmetry axes, generated by employing local 3-fold symmetry, originating from deep inside the PB pore and extending to its outer surface. We assign this to the shaft region of the fiber protein. This fiber shaft corresponds to a length of 90 Å and accommodates 5–6 beta-spiral repeats that are each about 13–15 Å along the fiber axis (Fig. 2c, d) in agreement with the 5.5 repeats predicted for the HAdV-35 fiber shaft (20). The density corresponding to the fiber knob was not visible. The ability of the penton base to adapt to large changes is striking. Conformational changes observed in the crystal structure may reflect early events in cell entry.

The C-termini of hexon subunits are involved in two different types of interactions. First, the C-termini stabilize the 3-fold junctions inside the capsid within each group of nine hexons (GON) in a facet. The C-terminal tail (green) (residue 944 to the last ordered residue 946, 949, or 951 in different subunits) forms an extra strand that interacts with a β-sheet in the V2 domain of the adjacent (clockwise; 3-fold related) hexon subunits in neighboring trimers (Fig. 3a, b).

The second type of interaction occurs between two C-terminal tails of hexon subunits with the two tails coming from adjacent (GONs) or with one of the tails coming from a peripentonal hexon. The two tails stack on top of each other. While there are no direct interactions between the C-terminal tails themselves, each interacts with residues in apposing hexon subunits primarily via hydrogen bonds. A highly ordered helix from protein VIII (residues 40–60) lies beneath and co-planar with these stacked C-termini further supporting the interface between hexon subunits at the capsid interior (Fig. 3a, c). In contrast to the C-termini, none of the N-termini of the hexons are involved in “direct” inter-hexon interactions. They are; however, involved in critical interactions with the cement proteins thus indirectly stabilizing the inter-hexon associations (detailed below).

The contiguous shell of the Ad35F capsid contains four cement proteins, IIIa, VI, VIII and IX that play significant roles in stabilizing the virion. Their locations have been tentatively assigned to the outer and inner surface of the capsid based on their copy number, cryoEM and biochemical analysis (12,14,21). We did not observe significant side-chain densities needed to definitively assign their sequence with the exception of VIII (see below). The triskelion-like structures, formed by N-terminal regions of three protein IX subunits (12,13) are located at four different positions per facet (Fig. 1) and stabilize the 3-fold GON junctions on the capsid exterior. The Ad35F crystal structure revealed a very well ordered 4-helix bundle, 80 Å in length, that is located on the capsid exterior between hexon-4 of one GON and hexon-2 of the neighboring GON (molecule in blue; Fig. 1a, b). Early cryoEM analyses (12,22) tentatively assigned density at this location to IIIa, which is the largest cement protein (63 kDa) in the HAdV capsid shell. However, a recent 6 Å resolution cryoEM analysis revealed the coiled coil shape of this density and led to the alternate hypothesis that this region might correspond to the C-termini of four IX molecules (14). This assignment to protein IX was also suggested by cryoEM analysis of Ad vectors with peptide tagged IX (23). Interestingly, the X-ray structure revealed that two of the helices in this 4-helix bundle appear to be connected at one end (Fig. S4a inset). This finding as well as the different distances observed from the visible ends of the (trimeric) triskelions of protein IX to the nearest helix of the (tetrameric) four-helix bundle raises the question as to whether the helical bundle is formed by 4 C-terminal helices of IX. Another possibility is that this helical bundle represents a domain of IIIa as originally proposed. A higher resolution density map will be required to definitively assign an amino acid sequence to this region.

The Ad35F structure also revealed multiple helices, organized primarily as two domains (Fig. S4b), on the inside of the virus capsid at the vertex region. The connectivity between these helices is not clear. While this region has been tentatively assigned as IIIa based on a cryoEM analysis (14), it is possible that at least some of these helices could correspond to the membrane lytic VI molecule (24) that participates in endosomalysis and whose N-terminal 80 residues have a high degree of alpha helical content. The helical domain, closest to the vertex, “cements” the contacts between two peripentonal hexons while the second domain appears to interact with the base of one peripentonal hexon. There is also a helix layered on top of one the molecules of VIII (A) (Fig. S4b). This helix along with two other short helices could belong to yet another cement protein. Interestingly, difference maps also showed that all of the hexon cavities are filled with electron density (Fig. S5), suggesting that at least part of the putative protein VI molecules could be sequestered inside the hexon trimers as previously suggested (25). These densities could account for over 200 VI molecules present in the HAdV capsid.

The HAdV particle contains 120 copies of protein VIII, a key “cement” protein, that has been tentatively assigned to the interior of the capsid based on its copy number and predicted alpha helical content (12,14). Our X-ray structure confirmed the location of VIII and provided more detailed information on its interactions with nearby hexon proteins (Fig. 4). We fit the VIII sequence into the electron density based on multiple criteria including the presence of a single predicted alpha helix, the location of key proline residues associated with a prominent U-shaped bend in the central portion of the VIII segment and the direction of the densities for the residues with long side chains (facing towards the N-terminus of the helix) in the sharpened maps. The ordered part of VIII molecule has an extended fold with an end-to-end span of 83 Å, starting with a helix of ~20 residues followed by a distinct inverted U-shaped structure and succeeded by an extended polypeptide chain (Fig. 4a). Furthermore, a large portion of the aligned sequence (residues 37–90) exhibited favorable side chain interactions with the residues from the nearby hexon subunits (Fig. 4c, d). Fifty-four residues of the mature form of VIII, resulting from cleavage by the virus cysteine protease, are visible at two independent locations in the electron density maps. The two structurally distinct VIII molecules (A and B) closely trace the base of individual hexons (inside) along the outer edge of the group of nine (GON) hexons and

mediate the interactions between GONs as well as between peripentonal hexons (Fig. 4b). Each VIII molecule in the Ad35F particle interacts with the N-termini of 3 subunits of hexon trimers related by local 3-fold symmetry. One of the protein VIII molecules, designated A, is located close to vertex region and interacts with two peripentonal hexons, while the second one, designated B, closely interacts with hexon-4 and hexon-3' (Fig. 3a, 4b). The ordered parts of each of these molecules closely associate with 3 hexon trimers.

Specifically, residues Ile41 and Ile54 in the N-terminal leg of the VIII molecule (A), mediate non-polar interactions with Pro7 and flanking residues at the N-terminus of a peripentonal hexon (hexon1') (Fig. 4b) and hexon-4 in the reference icosahedral asymmetric unit respectively (Fig. 4b, c). The inverted U-shaped kink comprising VIII residues 63–77 interacts with N-terminal residues 1–7 of one of the subunits of another peripentonal hexon (hexon-1) (Fig. 4d). Thus VIII molecule-A staples two peripentonal hexons with hexon-4. Likewise, the second VIII molecule-B mediates associations between three hexons, hexon-2' of a neighboring GON with hexons-3' and 4 from the reference GON using the quasi-equivalent interactions as described for VIII molecule-A (Fig. 4b–d).

The Ad35F structure provides insights into the virus-host interactions. While inter-hexon contacts are extensive and are augmented by the cement proteins, the interactions between the penton base and peripentonal hexons are rather tenuous (Fig. S6). This would favor efficient capsid disassembly and release of the penton complex during cell entry. The crystal structure of the entire HAdV particle also provides an initial assessment of the folds and interactions of cement proteins with the hexon subunits. Improved knowledge of HAdV assembly from its individual capsid proteins could lead to the development of novel antiviral strategies to block infection at multiple cell entry steps and facilitate the development of HAdV vectors with improved tissue targeting.

Supplementary Material

Refer to Web version on PubMed Central for supplementary material.

Acknowledgments

The authors express their deep gratitude to John E. Johnson for his advice and guidance during all phases of the structure determination and for reading the manuscript. We appreciate the outstanding technical support from Tina-Marie Mullen and Lance Gritton for vector production. Authors also acknowledge Sangita Venkataraman for her help with the early crystallization setups of HAdV, Irimpan Mathews of SSRL for his initial help with the data collection and Wladek Minor and Iwona Minor for generously providing the larger version of SCALEPACK program. We also thank Erica Ollmann-Saphire and Jason G. Smith for their comments on the manuscript and Theresa McCarthy for preparation of this paper. We also gratefully acknowledge Robert Fischetti, Nukri Sanishvili and other members at GM/CA CAT for discussions and technical support. GM/CA CAT has been funded in whole or in part with Federal funds from the National Cancer Institute (Y1-CO-1020) and the National Institute of General Medical Science (Y1-GM-1104). The use of the Advance Photon Source was supported by the U.S. Department of Energy, Basic Energy Sciences, Office of Science (contract No. DE-AC02-06CH11357). The coordinates of Ad35F crystal structure have been deposited in the Protein Data Bank (PDB) with the identification code 1VSZ. This work was supported by NIH grants R01 AI070771 to V.S.R., HL054352 and EY011431 to GRN, and AI042929 to PLS. This is manuscript # 20538 from The Scripps Research Institute.

References and Notes

1. Butt AL, Chodosh J. Adenoviral keratoconjunctivitis in a tertiary care eye clinic. Cornea 2006;25:199–202. [PubMed: 16371782]
2. Gordon YJ, Araullo-Cruz TP, Johnson YF, Romanowski EG, Kinchington PR. Isolation of human adenovirus type 5 variants resistant to the antiviral cidofovir. Invest Ophthalmol Vis Sci 1996;37:2774–2778. [PubMed: 8977495]

3. Hilleman MR, Werner JH. Recovery of new agent from patients with acute respiratory illness. Proc Soc Exp Biol Med 1954;85:183–188. [PubMed: 13134329]
4. Metzgar D, Osuna M, Kajon AE, Hawksworth AW, Irvine M, et al. Abrupt emergence of diverse species B adenoviruses at US military recruit training centers. J Infect Dis 2007;196:1465–1473. [PubMed: 18008225]
5. Hoffman JA. Adenoviral disease in pediatric solid organ transplant recipients. Pediatr Transplant 2006;10:17–25. [PubMed: 16499582]
6. Lenaerts L, De Clercq E, Naesens L. Clinical features and treatment of adenovirus infections. Rev Med Virol 2008;18:357–374. [PubMed: 18655013]
7. Edelstein ML, Abedi MR, Wixon J, Edelstein RM. Gene therapy clinical trials worldwide 1989–2004-an overview. J Gene Med 2004;6:597–602. [PubMed: 15170730]
8. Henry TD, Grines CL, Watkins MW, Dib N, Barbeau G, et al. Effects of Ad5FGF-4 in patients with angina: an analysis of pooled data from the AGENT-3 and AGENT-4 trials. J Am Coll Cardiol 2007;50:1038–1046. [PubMed: 17825712]
9. van Raaij MJ, Mitraki A, Lavigne G, Cusack S. A triple beta-spiral in the adenovirus fibre shaft reveals a new structural motif for a fibrous protein. Nature 1999;401:935–938. [PubMed: 10553913]
10. Zubieta C, Schoehn G, Chroboczek J, Cusack S. The structure of the human adenovirus 2 penton. Mol Cell 2005;17:121–135. [PubMed: 15629723]
11. Rux JJ, Burnett RM. Type-specific epitope locations revealed by X-ray crystallographic study of adenovirus type 5 hexon. Mol Ther 2000;1:18–30. [PubMed: 10933908]
12. Fabry CM, Rosa-Calatrava M, Conway JF, Zubieta C, Cusack S, et al. A quasi-atomic model of human adenovirus type 5 capsid. EMBO J 2005;24:1645–1654. [PubMed: 15861131]
13. Saban SD, Nepomuceno RR, Gritton LD, Nemerow GR, Stewart PL. CryoEM structure at 9A resolution of an adenovirus vector targeted to hematopoietic cells. J Mol Biol 2005;349:526–537. [PubMed: 15890367]
14. Saban SD, Silvestry M, Nemerow GR, Stewart PL. Visualization of alpha-helices in a 6-angstrom resolution cryoelectron microscopy structure of adenovirus allows refinement of capsid protein assignments. J Virol 2006;80:12049–12059. [PubMed: 17005667]
15. Smith TA, Idamakanti N, Rollence ML, Marshall-Neff J, Kim J, et al. Adenovirus serotype 5 fiber shaft influences in vivo gene transfer in mice. Hum Gene Ther 2003;14:777–787. [PubMed: 12804140]
16. Reddy VS, Natchiar SK, L. G, Mullen TM, Stewart PL, et al. Crystallization and preliminary X-ray diffraction data analysis of Human Adenovirus. Virology. 2010 doi:10.1016/j.virol.2010.03.028.
17. Materials and methods are available as supporting material on Science Online.
18. Fuschiotti P, Schoehn G, Fender P, Fabry CM, Hewat EA, et al. Structure of the dodecahedral penton particle from human adenovirus type 3. J Mol Biol 2006;356:510–520. [PubMed: 16375921]
19. Von Seggern DJ, Chiu CY, Fleck SK, Stewart PL, Nemerow GR. A helper-independent adenovirus vector with E1, E3, and fiber deleted: structure and infectivity of fiberless particles. J Virol 1999;73:1601–1608. [PubMed: 9882366]
20. Shayakhmetov DM, Lieber A. Dependence of adenovirus infectivity on length of the fiber shaft domain. J Virol 2000;74:10274–10286. [PubMed: 11044071]
21. van Oostrum J, Burnett RM. Molecular composition of the adenovirus type 2 virion. J Virol 1985;56:439–448. [PubMed: 4057357]
22. Stewart PL, Fuller SD, Burnett RM. Difference imaging of adenovirus: bridging the resolution gap between X-ray crystallography and electron microscopy. EMBO J 1993;12:2589–2599. [PubMed: 8334984]
23. Campos SK, Barry MA. Current advances and future challenges in Adenoviral vector biology and targeting. Curr Gene Ther 2007;7:189–204. [PubMed: 17584037]
24. Wiethoff CM, Wodrich H, Gerace L, Nemerow GR. Adenovirus protein VI mediates membrane disruption following capsid disassembly. J Virol 2005;79:1992–2000. [PubMed: 15681401]
25. Silvestry M, Lindert S, Smith JG, Maier O, Wiethoff CM, et al. Cryoelectron microscopy structure of adenovirus type 2 temperature-sensitive mutant 1 reveals insight into the cell entry defect. J Virol 2009;83:7375–7383. [PubMed: 19458007]

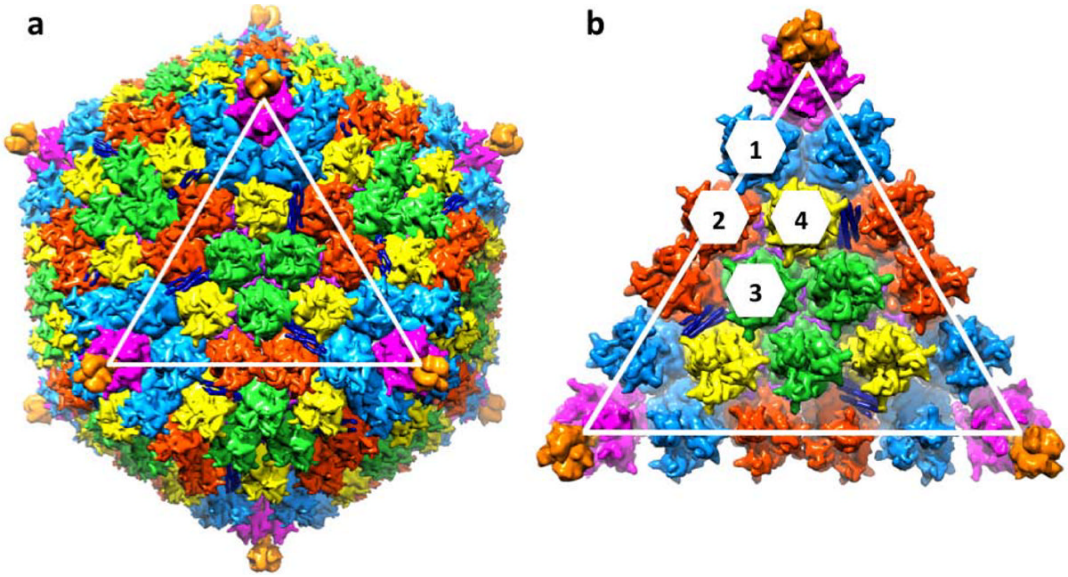

Figure 1.

Surface rendering and subunit associations of Ad35F. (a) Outer capsid viewed down the particle 3-fold axis with a facet circumscribed by the white triangle. (b) A zoom in view of the single facet. The icosahedral asymmetric unit is composed of one of the PB (pink) subunits and 4 hexon trimers (cyan(1), red(2), green(3), yellow(4)). Cement proteins on the outside of the capsid are shown in blue (4-helix bundle) and magenta (IX triskelion). Twelve hexon trimers occupy one facet of the Ad35F capsid; however, a total of 18 hexons are shown for clarity. A model of the trimeric fiber docked into each penton base is shown in orange.

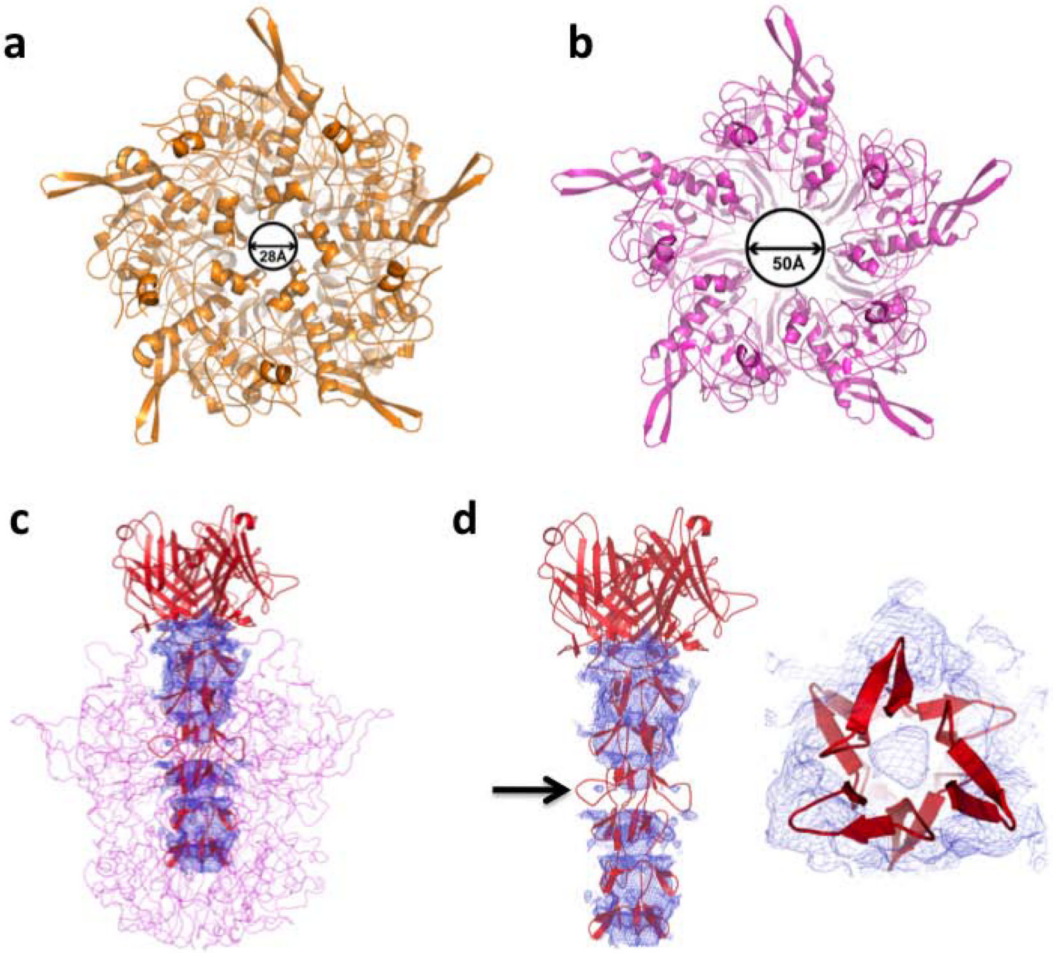

Figure 2.

Structure of the penton complex. (a) The structure of the isolated PB shown in gold (10) with a maximum pore diameter of 28 Å. (b) The structure of the PB in the Ad35F particle shown in magenta with a maximum pore dimension of 50 Å. (c) Panel showing the 3-fold averaged difference (F_o–F_c) electron density (in blue, contoured at 2.5σ) corresponding to the fiber molecule along the 5-fold axis of the PB, shown as magenta trace. Structure of the HAdV-35 fiber molecule based on the partial HAdV-2 fiber structure (9), represented as ribbon diagram (red) and fitted into the difference density. (d) A vertical view of the fit of the fiber shaft to the difference density (left). The flexible 3rd repeat of the shaft is indicated by an arrow. A view down the fiber axis showing the fit of one of the shaft repeats (right).

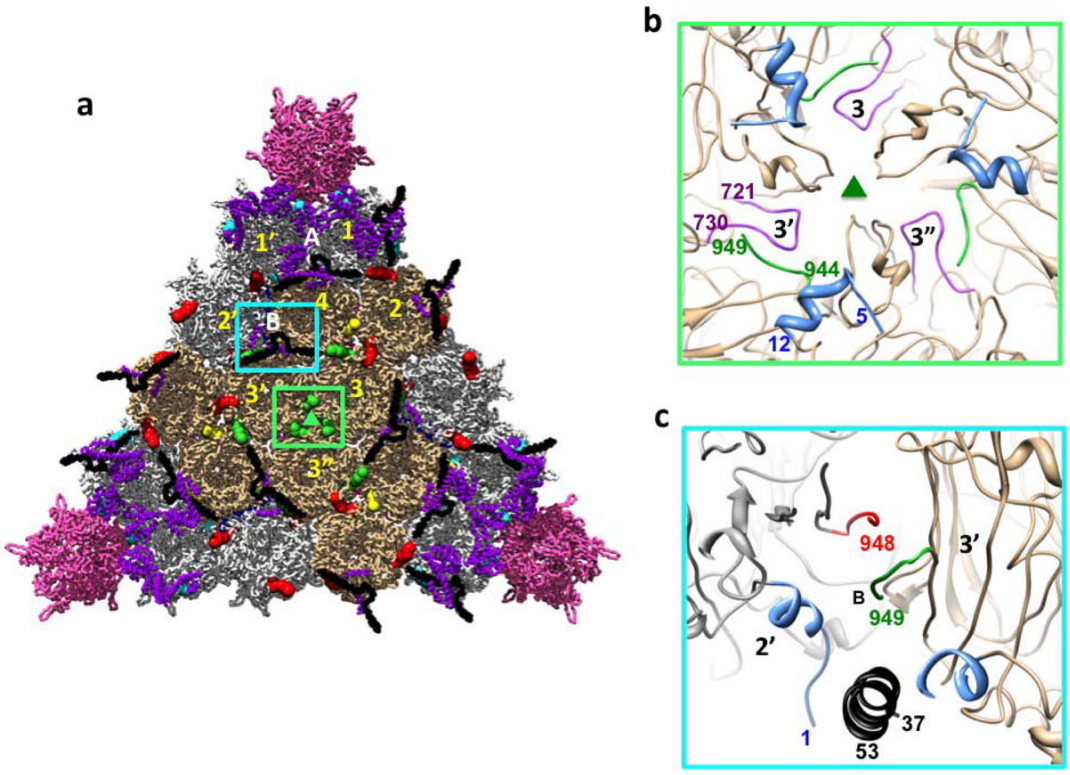

Figure 3.

Hexon associations at the inner capsid surface. (a) Inner surface of a facet showing the locations of hexon C-termini, shown as spheres according to the hexon color-coding used in Fig. 1a. Group of nine (GON) hexons in the facet are shown in tan color, while the rest of the hexons are shown in gray for clarity. VIII molecules are shown in black. PB subunits are shown in pink and additional cement proteins in purple. Structurally distinct locations (A and B) of VIII molecules as well as the 4 hexon trimers (1, 2, 3 and 4) of the icosahedral asymmetric unit are indicated. Hexons related by icosahedral symmetry are indicated with the prime/double prime symbols. (b) Formation of extended β-sheets by the hexon C-termini (green) with the EF-strands (aa 721–730; purple) of the V2 domain of the neighboring (clockwise) hexon subunit at the icosahedral 3-fold axis (triangle). (c) Stacking of the hexon C-termini (red and green) at the inter-GON interface with a helix from VIII (black). Hexon N-termini that interact with VIII are shown in powder blue.

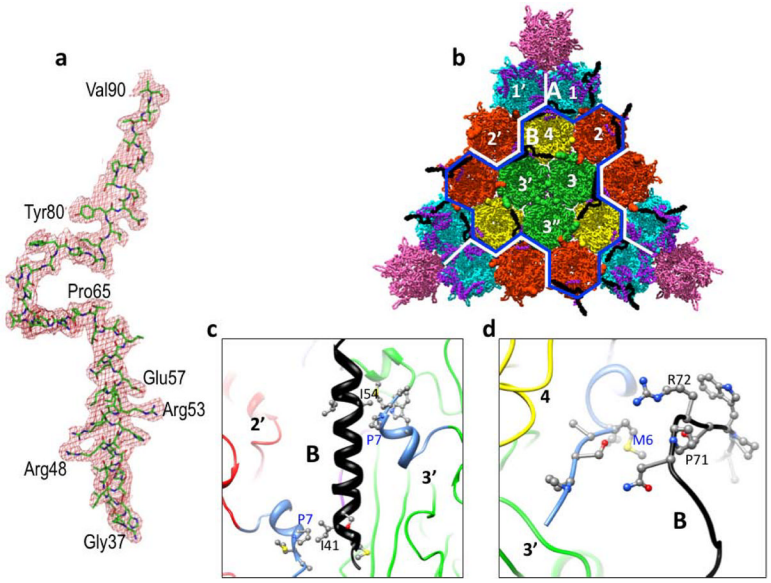

Figure 4.

Structure and interactions of pVIII with the hexons. (a) Display of $2F_o-F_c$ electron density (contoured at 1.0 σ) of the ordered part of a VIII molecule. (b) An interior view of the facet showing the locations of proteins VIII (black) and additional cement proteins (purple). An outline of the group of nine hexons (GONs) is shown by a thick blue line. A line trace corresponding to the location of three P30 molecules (in white) from PRD1 (9) is shown in comparison with protein VIII and in the context of the Ad35F structure. Hexons are color coded and numbered according to the scheme described in Fig. 1a and Fig. 4a respectively. (c) Non-polar interactions between a VIII helix (black) with the N-termini (powder blue) of two neighboring hexons viewed from the inside of the virus. (d) Close approach of the inverted U-shaped bend in VIII (black) to the N-terminus of a hexon subunit. However, the interactions of the U-shaped structure are not as close and specific as those mediated by the helix in panel c.